DECOMPOSITION OF THE LAPLACIAN FILTER OPERATOR FOR REVERSE TIME MIGRATION

XIN TIAN[1], SAMAN AZADBAKHT[2] and CHIYUAN REN[3]

[1] *Engineering College, Southwest Petroleum University, Chengdu 610500, P.R. China.*
tianxinrjx@163.com
[2] *Petroleum Systems Engineering, University of Regina, SK, Canada S4S 0A2.*
[3] *Science College, Southwest Petroleum University, Chengdu 610500, P.R. China.*

(Received April 24, 2017; revised version accepted May 15, 2018)

ABSTRACT

Tian, X., Azadbakht, S. and Ren, C.Y., 2018. Decomposition of the Laplacian filter operator for reverse time migration. *Journal of Seismic Exploration*, 27: 349-370.

Reverse time migration is considered as an effective approach to obtain the images of layers, but it usually produces some artifacts in the images. Applying a Laplacian filter is a conventional and effective approach to improve these images. In this work, the Laplacian operator is decomposed mathematically. Based on this decomposition, the reason why the Laplacian filter can improve images is investigated thoroughly, and the work part is identified. Then we discard the useless part and employ the work part to form a new imaging condition. At first, shown in a one-shot numerical experiment, the proposed imaging condition can simultaneously remove the low-and high-frequency artifacts effectively. Then, the Sigsbee2A velocity model is employed as a synthetic example to verify the proposed imaging condition. The numerical results show that the proposed imaging condition can effectively govern the principal energy in wave fields and damp artifacts in angle domain.

KEY WORDS: reverse time migration, imaging condition, Laplacian operator, artifact removal.

0963-0651/18/$5.00

INTRODUCTION

Due to employ two-way wave equation, reverse time migration (RTM) can image by all acoustic waves, such as reflections, refractions, diffractions, multiples, and evanescent waves (McMechan, 1983; Whitmore, 1983; Baysal et al., 1983). It allows RTM images layers without dip limitations and work better than other imaging methods, especially in complex structures (Li et al., 2013). RTM forward extrapolates source wave field from sources and backward extrapolates receiver wavefield from receivers, then an imaging condition is applied between them to form a depth image. To extrapolate wavefields and avoid numerical diffusion, high-order finite difference schemes must be employed, which are usually expensive and limited in practical applications. Due to rapid developments in computer hardware, such as Linux clusters and GPU cards, the computational complexity of RTM is no longer an insurmountable obstacle. Thus, in some complex structures with large velocity variations, RTM become a competitive imaging method.

Zero-lag cross-correlation imaging condition (CC) is first constructed by Claerbout (1971). It is simple and has correct kinematics, but it often produces high-amplitude, low-frequency noise near sharp interfaces and ground surface (Claerbout, 1985). Researchers have proposed many approaches to overcome the problem. These methods can be divided into three classes based on the applying time of methods: (1) pre-imaging methods, which modify extrapolation method of wave equation to suppress unwanted reflections; (2) in-imaging methods, which improve imaging condition to retain only the reflected wave energy; and (3) post-imaging methods, which filter the image by filter operators.

To denoise before applying imaging condition, modifying extrapolation process of wave equation is feasible method. One-way wave equation and smoothing velocity model are effective approaches, but it is at the cost of reducing imaging quality (Baysal et al., 1984; Zhang, 2007). Fletcher et al. (2005) induced a directional damping factor into the governing wave equation to suppress unwanted reflections. Liu et al. (2008) used anti-dispersion wave equation to suppress numerical dispersion and to denoise images. Yan et al. (2009) decomposed the wavefield into local plane waves, then cross-correlated them to image. Some researchers had attempted to modify the imaging condition directly to damping noise (Chattopadhyay and McMechan., 2008; Costa et al., 2009; Loewenthal et al., 1987; Sava et al., 2006; Suh et al., 2009). Normalization by the square of source illumination strength was developed to obtain correct reflection amplitudes (Claerbout,

1971), and normalization of the square of receiver illumination strength is also feasible (Kaelin and Guitton, 2006). Zhou and Schuster (2002) suggested using windowed CC to mute unwanted correlations. Liu et al. (2007, 2011) and Fei et al. (2010) decomposed the source and receiver wavefields into two wavefields that propagate in opposite directions. Meanwhile, CC has also been modified to suppress the correlation between the source and receiver wavefields that propagate in parallel directions. Yoon et al. (2006) employed the Poynting vector to mute these cross-correlations, where the angle between the Poynting vectors was greater than a given angle, such as 120°. Ren et al. (2015) combined the two approaches of Liu et al. and Yoon et al. to obtain better images. Save et al. (2006, 2011) proposed a generalized imaging condition in which space-shifts and time-shifts are induced to implement angle image. After applying imaging condition, filters are usually used to obtain better images. Mulder and Plessix (2003) used a high-pass filter to suppress low-frequency noise.

The Laplacian operator is a derivative operator which is commonly used in image processing for edge detection and motion estimation applications. In the field of image process, the Laplacian operator is approximated to a matrix named as discrete Laplace operator matrix by finite-difference method (Reuter et al., 2009). Meanwhile, because interfaces between layers are most concerned by the seismic interpreter, the Laplacian operator usually is employed to improve the images conducted by migration (Zhang and Sun, 2009; Schuster and Dai, 2010). Guitton (2007a,b) used a variety of filter operations to suppress noise in the wave number domain, including differential filter, the Laplacian filter, and least squares filter et al.

In this investigation, we focus on the Laplacian filter in RTM, and analyze the reason why the Laplacian filter can improve images based on a mathematical decomposition of the operation. Then, a detailed analysis is performed to identify the work part of the Laplacian filter. Based on the decomposition, the useless part is discarded, and the effective part is extracted to form a new imaging condition. Numerical investigation shows that the advantages of the Laplacian filter can be utilized, and its weaknesses are avoided. This paper is organized as follows. The first section presents the definition and algorithm of RTM and summarizes the principal denoising approaches. Decomposition of the Laplacian operator is then proposed, and the effective part is identified via theoretical analysis and numerical simulation. The proposed imaging condition is then verified numerically by comparing it with the zero-lag cross-correlation imaging condition in Sigsbee2A dataset. The last section presents some conclusions.

THEORY

Reverse Time Migration

Prestack RTM includes two key steps. At first, the source wavefield is extrapolated forward in time, and the receiver wavefield is simultaneously extrapolated backward in time. Then an imaging condition is applied to the two wavefields to form a depth image. In this study, the two-way scalar wave equation is employed to simulate wavefields. In 2D, the equation can be formulated as

$$\frac{\partial^2 p(X,t)}{\partial t^2} = c^2 \nabla^2 p(X,t) \tag{1}$$

where p is the wavefield pressure at a location X and time t, and c is the sonic velocity of media.

In RTM, source and receiver wavefields are independently extrapolated using the same wave eq. (1), then an imaging condition is applied between them. CC is a traditional imaging condition in RTM that is defined as zero-lag cross-correlation between the forward-propagated source wavefield and the backward-propagated receiver wavefield (Claerbout, 1971; Feng et al., 2015). The imaging condition can be expressed as

$$I(X) = \sum_{shots} \sum_{t} S(X,t) R(X,t) \tag{2}$$

where $I(X)$is the depth image at location X, and $S(X,t)$ and $R(X,t)$ are the source and receiver wavefields, respectively, at time t and location X. This imaging condition is sufficient for media with small impedance contrasts and simple geological structures.

The Laplacian filter for reverse time migration

Due to employ two-way wave equation in RTM, source and receiver wavefields cross-correlate along the entire path along wave passing through. So CC usually generates lots of large-amplitude, low-frequency noise near sharp interfaces. To attenuate these noises, several filter operators usually are employed. Filters are easier to use than these approaches in the pre-

imaging and in-imaging categories. Usually, only an additional filter operator is employed to transform the image. The unified expression could be formulated as

$$D(I(X)) = D(\sum_{shots}\int_0^{T_{\max}} S(X,t)R(X,t)dt) \quad , \tag{3}$$

where D is a filter operator. Due to the low-frequency properties of noise, high-pass filter is a direct approach to remove these noises (Mulder and Plessix, 2003). Moreover, for prestack seismic data, the coincidence between source wavefield and receiver wavefield will generate a sharp jump in the subsurface (Haney et al., 2005). For this reason, derivatives should be an effective tool for identifying these sharp jumps. Guitton et al. (2007) employed several filters to remove this noise, including derivative filtering, Laplacian filtering and least-squares filtering. The Laplacian filter was also used by Pratt (1978) and Youn et al. (2001) to enhance the interfaces between layers. Youn et al. (2001) concluded that the performance of Laplacian operator was better than divergence operator. Claerbout (1998) factored the Laplacian operator into minimum-phase filters using a helix derivative. The approach does not affect dips but maybe change the phase of reflections. In this study, we follow their steps and make some new investigation on the Laplacian operator for RTM.

DECOMPOSITION OF THE LAPLACIAN OPERATOR FOR REVERSE TIME MIGRATION

With no loss of generality, we only illustrate our theory and algorithm in 2D. If a Laplacian filter is applied on an image, the following expression could be obtained

$$\nabla^2(I(X)) = \nabla^2(\sum_{shots}\sum_{t} S(X,t)R(X,t)) \quad , \tag{4}$$

where $\nabla^2 = \frac{\partial^2}{\partial x^2} + \frac{\partial^2}{\partial y^2}$. By putting ∇^2 inside the summation, we obtain

$$\nabla^2(I(X)) = \sum_{shots}\sum_{t} \nabla^2(S(X,t)R(X,t)) \quad . \tag{5}$$

Decompose the Laplacian operator using (A-3), which is proved in the Appendix.

$$\begin{aligned}\nabla^2(I(X)) &= \sum_{shots}\sum_{t}\nabla^2(S,R)\cdot(R,S)+2\nabla(S)\cdot\nabla(R)\\ &= \sum_{shots}\sum_{t}\nabla^2(S,R)\cdot(R,S)+\sum_{shots}\sum_{t}2\nabla(S)\cdot\nabla(R)\\ &= \sum_{shots}\sum_{t}DeLap1+\sum_{shots}\sum_{t}DeLap2\end{aligned}, \qquad (6)$$

where

$$\begin{aligned}DeLap1 &= \nabla^2(S,R)\cdot(R,S)\\ DeLap2 &= 2\nabla(S)\cdot\nabla(R)\end{aligned}, \qquad (7)$$

where the symbol · expresses the inner product between vectors. Thus, the post-imaging condition the Laplacian filter can be decomposed into two in-imaging conditions: *DeLap*1 and *DeLap*2.

To verify the performance of the two decomposed parts, we employ a four-layer velocity model to test them firstly. The model is simple and only contains vertical velocity gradient, as depicted in Fig. 1. The model domain is 16,000 ft wide and 8,000 ft high. And the model is meshed to 400 by 200 grids; i.e., the spatial grid increments are set to 40 ft in both vertical and horizontal directions. The velocity of top layer is 7000 ft/sec, and the velocity of each subsequent layer increases by 500 ft/sec. One source is set in the middle of ground surface, and all 200 receivers are distributed evenly on the surface. Time increment is set to 0.75 ms, which could ensure computational stability and reduce grid dispersion. A Ricker wave with dominant frequency 25 Hz is employed to simulate the amplitude of source based on time. A 2D eight-order finite difference schedule is employed to extrapolate wavefields, and perfectly matched layer (PML) boundary condition is employed to absorb the energy that passes through boundaries. At the same time, the synthetic datasets are preprocessed before migration by muting the direct wave to reduce artifacts (Chang and McMechan, 1986).

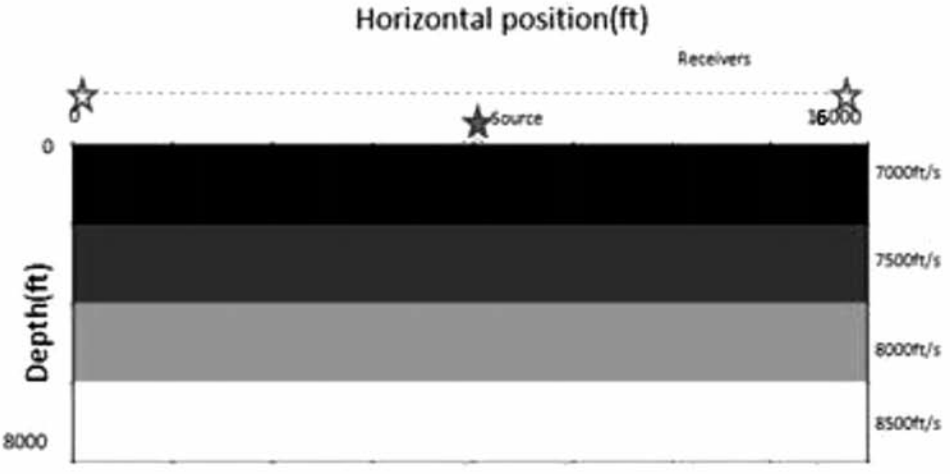

Fig. 1. Four-layer velocity model.

Depicted in Fig. 2 are the images conducted by CC. Fig. 2(a) shows the original image, while Fig. 2(b) shows the image filtered by the Laplacian operator. The image conducted by CC is clear, but it has several short comings. Firstly, serious low-frequency noise above the top reflector contaminates the shallow image. Secondly, the images of reflectors that are enclosed by the right box are higher than their true locations. Furthermore, the greater the angle of incidence is, the more serious the misfits are. It maybe leads to incorrect seismic interpretations. Thirdly, several butterfly knots (left box) appear between the layers. Fig. 2(b) shows the image filtered by the Laplacian operator. Most of the low-frequency noise has been removed, and the interfaces have been enhanced, which makes the image more distinct. However, the artifacts that are enclosed by the two boxes are still retained in the image. Some of the artifacts above the top reflector are enhanced and form high-frequency noises. This verifies that the Laplacian filter can remove low-frequency noise at the cost of increasing some high-frequency noises.

Fig. 3 shows the performances of *DeLap*1 and *DeLap*2. Fig. 3(a) depicts the image conducted by *DeLap*1. The image shows little improvement compared with the figure conducted by CC. It still contains shallow noise above the top reflector, butterfly knots between the layers and misfits of the reflectors. Thus, *DeLap1* cannot improve the image. It indicates that the first decomposition part (*DeLap*1) is not the principal reason why the Laplacian operator can effectively improve images. Fig. 3(b) shows the image conducted by *DeLap*2, in which much of the noises in the two boxes

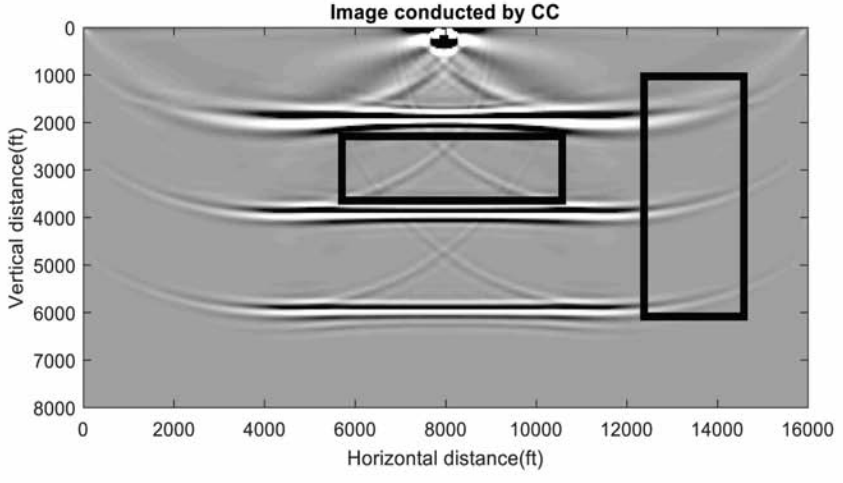

(a)

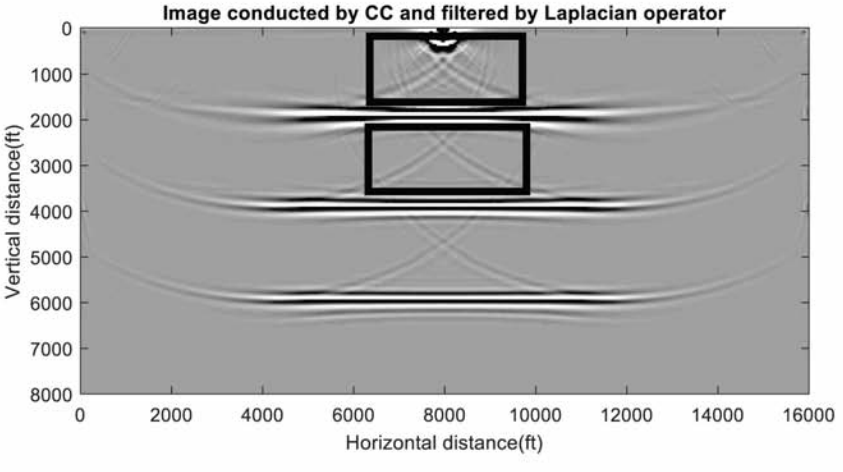

(b)

Fig. 2. Images conducted by zero-lag cross-correlation imaging condition. (a) Original image; (b) filtered by the Laplacian operator.

has been removed. Butterfly knots between the layers have been attenuated (left box), furthermore, the misfit images of the reflectors have been suppressed (right box). It indicates, the second decomposition part (*DeLap*2) can effectively remove these artifacts. However, it cannot remove the shallow noise above the top reflector. Fig. 3(c) shows the summation of the two images conducted by *DeLap*1 and *DeLap*2. This image is similar as the image conducted by CC and filtered by the Laplacian operator except some numerical error, which verifies our mathematical decomposition.

FURTHER DECOMPOSITION OF THE LAPLACIAN OPERATOR

Decomposition of *DeLap*1

Furthermore, by inserting the wave equation [eq. (1)] into eq. (3), we obtain

$$\begin{aligned} DeLap1(S,R) &= \nabla^2(S,R)\cdot(R,S) \\ &= \frac{1}{c^2}\partial_{tt}(S,R)\cdot(R,S) \\ &= \frac{1}{c^2}(S_{tt}R + SR_{tt}) \end{aligned} \quad . \tag{8}$$

It shows, *DeLap*1 is the product between the second-order time derivative of a wavefield and the another wavefield. To further illustrate the essence of the expression, we use a second-order center difference to discretize these derivatives. We obtain

$$\begin{aligned} S_{tt}R &\approx \frac{1}{\Delta t^2}(S(t+\Delta t) + S(t-\Delta t) - 2S(t))R(t) \\ SR_{tt} &\approx \frac{1}{\Delta t^2}S(t)(R(t+\Delta t) + R(t-\Delta t) - 2R(t)) \end{aligned} \quad . \tag{9}$$

By summing the two equations, we obtain

$$\begin{aligned} S_{tt}R + SR_{tt} \approx \frac{1}{\Delta t^2}&(S(t+\Delta t)R(t) + S(t-\Delta t)R(t) \\ &+ S(t)R(t+\Delta t) + S(t)R(t-\Delta t) - 4S(t)R(t)) \end{aligned} \quad . \tag{10}$$

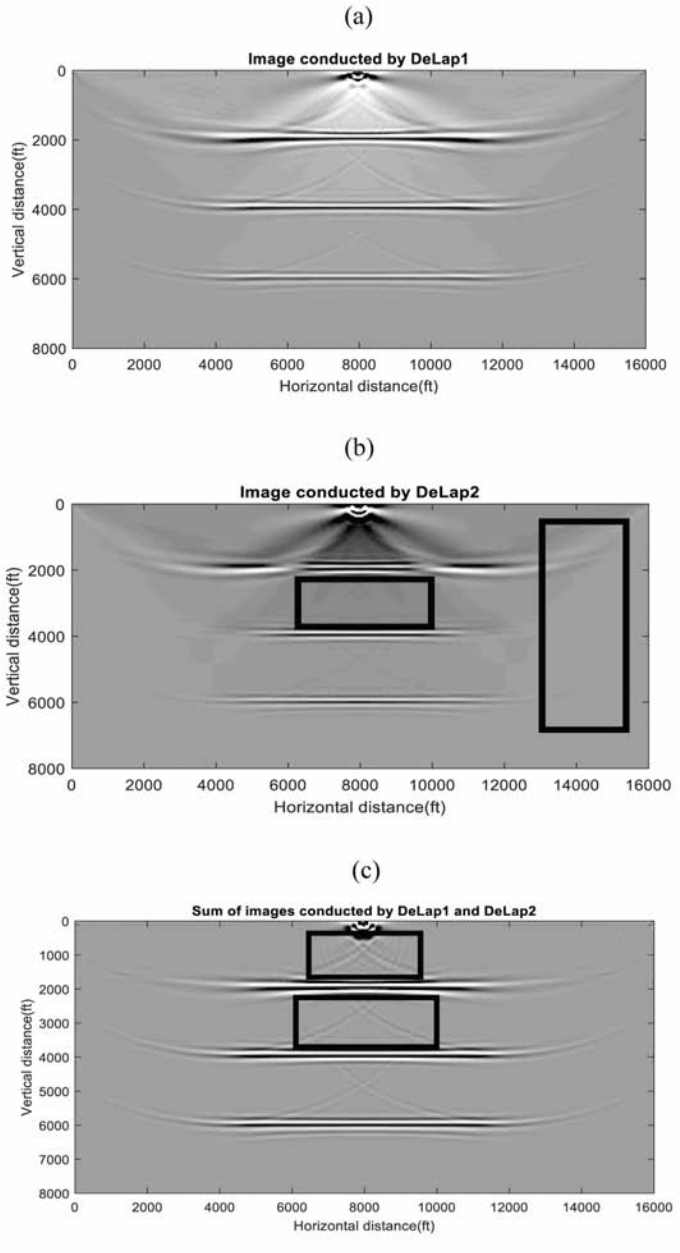

Fig. 3. Images conducted by the decomposed Laplacian operator. (a) Image conducted by the first part of the decomposition of the Laplacian filter; (b) image conducted by the second part of the decomposition of the Laplacian filter; (c) summation of (a) and (b).

The products $S(t+\Delta t)R(t)$, $S(t-\Delta t)R(t)$, $S(t)R(t+\Delta t)$ and $S(t)R(t-\Delta t)$ resemble the time-shift imaging condition, which was suggested by Sava et al. (2006, 2011). Thus, *DeLap*1 can be considered as the difference between zero-lag CC image and time-shift image. The numerical simulation with four-layer velocity model shows that it does not improve the image. Thus, we claim that the first part of the decomposition (*DeLap*1) is not the key reason that the Laplacian filter can improve the image conducted by CC.

Decomposition of *DeLap*2

*DeLap*2 is the inner product of the gradients of source wavefield and receiver wavefield, which is formulated as follows:

$$\begin{aligned} DeLap2(S,R) &= 2\nabla S \cdot \nabla R \\ &= 2Cos(\nabla S, \nabla R)\|\nabla S\|\|\nabla R\| \\ &= 2DeLap21 \cdot DeLap22 \end{aligned} \tag{11}$$

where $DeLap21 = Cos(\nabla S, \nabla R)$, and $DeLap22 = \|\nabla S\| \cdot \|\nabla R\|$. $DeLap21$ is the cosine of the angle between the gradients of source and receiver fields, and $DeLap22$ is the product of the norms of the gradients of source and receiver wavefields. $DeLap21$ can be considered as weight with respect to the angle. Therefore, $DeLap2$ employs the information of angle domain to image.

We explain the meaning of weight *DeLap*21 by using Poynting vector. Poynting vector commonly describes the energy flux density in wavefield, which can be considered as a ray direction and is expressed as

$$F(X,t) = -\nabla p(X,t)\frac{dp(X,t)}{dt}p(X,t) \quad , \tag{12}$$

where p is the amplitude of wavefield, and $F(X,t)$ is the Poynting vector at location X and time t. Thus, *DeLap*21 can be expressed by Poynting vector as

$$DeLap21 = Cos(\nabla S, \nabla R) = Cos(-F_S \cdot \frac{dt}{S \cdot dS}, -F_R \cdot \frac{dt}{R \cdot dR})$$
$$= sign(\frac{dt}{S \cdot dS}) sign(\frac{dt}{R \cdot dR}) \cos(F_S, F_R) \quad (13)$$

If the velocity model is accurate, then $\frac{dt}{S \cdot dS}$ and $\frac{dt}{S \cdot dS}$ should have the same sign. Therefore,

$$DeLap21 = Cos(\nabla S, \nabla R) = Cos(F_S, F_R) \quad . \quad (14)$$

Thus, *DeLap*21 is equal to the cosine of the angle between the Poynting vectors of source and receiver wavefields, which means that *DeLap*2 is weighted by the propagating direction of waves. Therefore, *DeLap*21 is an angle-domain filter operator (Liu et al., 2011; Yoon and Marfurt, 2006; Haney et al., 2005; Costa et al., 2009; Zhang and Sun, 2008; Diaz and Sava, 2012; Yan and Xie, 2009; Xie et.al, 2014). It is similar as applying Poynting vector on zero-lag cross-correlation imaging condition, which was proposed by Yoon and Marfurt (2006), and applying obliquity-correction operator that was proposed by Costa et al. (2009). In the former research, cross-correlation is muted beyond a given angle by Poynting vector. And in the latter research, the amplitude is corrected by an obliquity-angle. However, the attenuation in angle domain is implemented automatically in *DeLap*2. Its function in practice will be elaborated in the following.

We denote the angle between the ray directions (i.e., Poynting vector) in source and receive wavefield as θ. Therefore, θ is the angle between the incidence rays and the reflection ray. It should be twice of the incidence angle. If the incidence ray is from the normal direction, i.e., the incidence angle is equal to zero, then the cross-correlation of source and receiver wavefields will not be attenuated. If the incidence ray is not from the normal direction, the cross-correlation will be attenuated based on eq. (11). Furthermore, the greater the angle is, the greater the attenuation is.

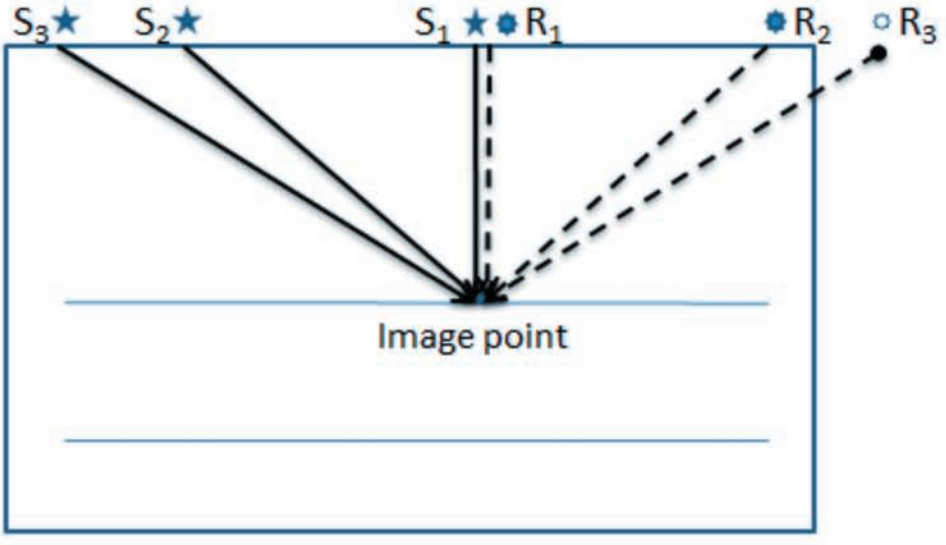

Fig. 4. Three pairs of shots and receivers with different angles of incidence. The third receiver (R3) is a virtual receiver.

To explain the reason why the attenuation can improve images, three pairs of incidence rays and reflector rays are shown in Fig. 4. In this figure, the three shots S1, S2 and S3 contribute to the imaging point I with different incidence angles; R1, R2 and R3 are the receiver points in the reflection ray paths. The incidence angle of the first pair (S1 and R1) is equal to 0, so the image conducted by them is the original value without any attenuation; the second pair (S2 and R2) has a small incidence angle, so the image conducted by them is attenuated based on the incidence angle; the third pair (S3 and R3) has a large incidence angle, so the image conducted by them is attenuated significantly. As depicted, the third receiver (R3) is beyond the extent of the computation domain, i.e., it is a virtual receiver but a real receiver. R3 does not exist, so it is impossible for the third shot (S3) to form a correct image at point I. Thus, artifacts appear. These artifacts have high frequencies and are difficult to be removed. In practice, the number of receivers, the offset of receivers, and the computational domain are usually limited. Thus, due to these limitations, distortion in image is inevitable. Because receivers are usually set near shots, the image

conducted by rays with small incidence angles is more credible, which implies that the attenuation based on incidence angle is reasonable and effective. It can also explain the effect of Laplacian operator, and indicates that *DeLap*2 can work better. Another aspect that must be further investigated is that: if the angle θ is greater than 90°, a negative value will be obtained. When θ is equal to 180°, the direction of incidence ray is opposite to that of reflector ray, which usually indicates that it is not a reflection point but rather a passing point in propagation path. Yoon and Marfurt suggested that it should be muted. Based on this idea, *DeLap*2 could be revised as

$$DeLap2R = \delta(DeLap2 > 0) \cdot DeLap2 \tag{15}$$

where δ is the Dirichlet function. In this formulation, cross-correlation in which incidence angle is greater than 45° will be muted. *DeLap*2R can remove the cross-correlation along wave propagation path, so most of low-frequency noises can be suppressed.

We verify the theoretical conclusion via a numerical simulation using the 2D velocity model and datasets that had been used in the previous section. At first, several snapshots of the imaging process are used to illustrate the results. Fig. 5 shows the snapshots of source and receiver wavefields at a time of 0.7 s, where the receiver wavefield is more complex than the source wavefield. The back-scattering waves usually cross-correlate with the source wavefield to form artifacts from all directions, which maybe contaminate the final image. Figs. 6(a) and (b) show the images conducted by CC and *DeLap*2R, respectively. It is clear that *DeLap*2R could images the reflectors with fewer artifacts, and most of the unwanted cross-correlation along the wave propagation path is removed. Fig. 7 shows the final image conducted by *DeLap*2R for one-shot dataset. Comparison between Figs. 2 and 3 shows that *DeLap*2R not only removes most of low-frequency noises, but also removes high-frequency noises. However, these high-frequency noise was usually enhanced, if the Laplacian operator is applied directly, as shown in Fig. 3.

An additional comparison is shown in Fig. 8, where we depict a vertical test line from Fig. 2(b) and Fig. 7 at horizontal distance 9000 ft. In these figures, both CC and *DeLap*2R can image the reflectors at the correct locations, but *DeLap*2R produces less noise, especially in the shallow layer. At the same time, the images of reflectors have a higher contrast ratio when *DeLap*2R is employed, which implies that *DeLap*2R can image the reflectors better.

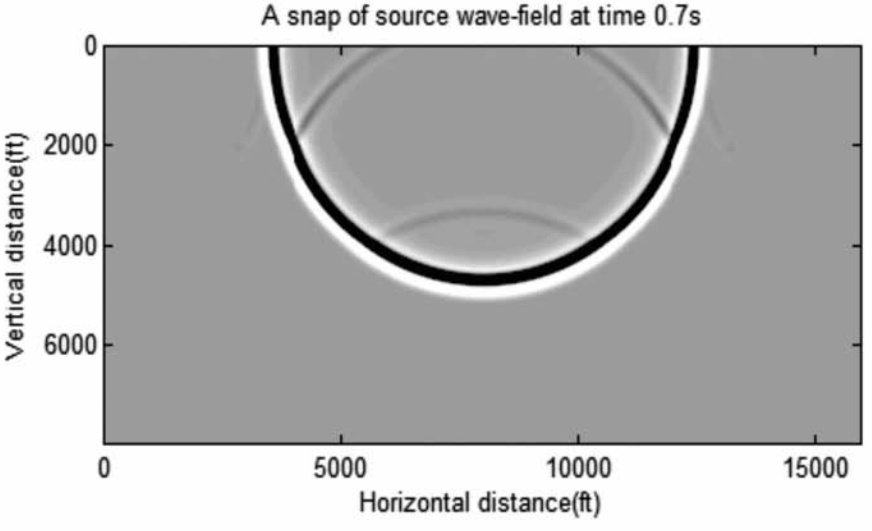

(a)

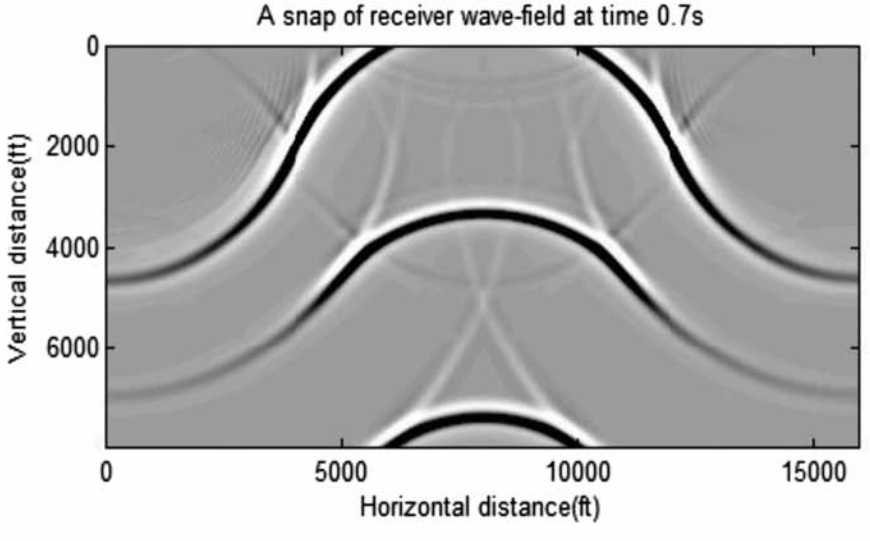

(b)

Fig. 5. Snapshots of the source and receiver wavefields at time 0.7 s.

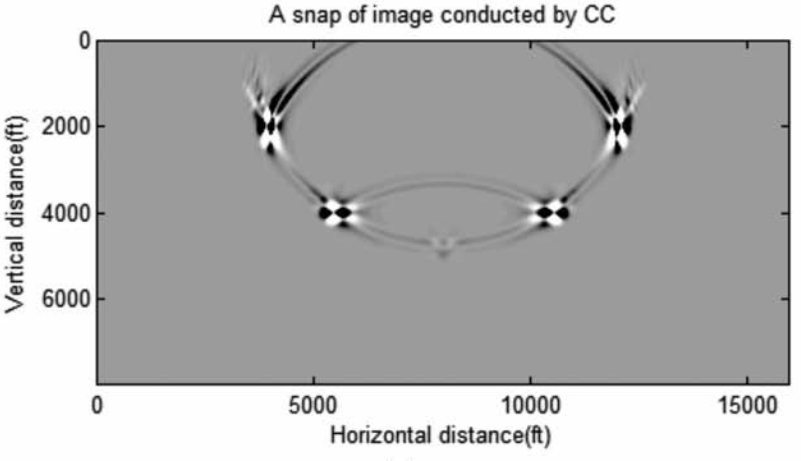

(a)

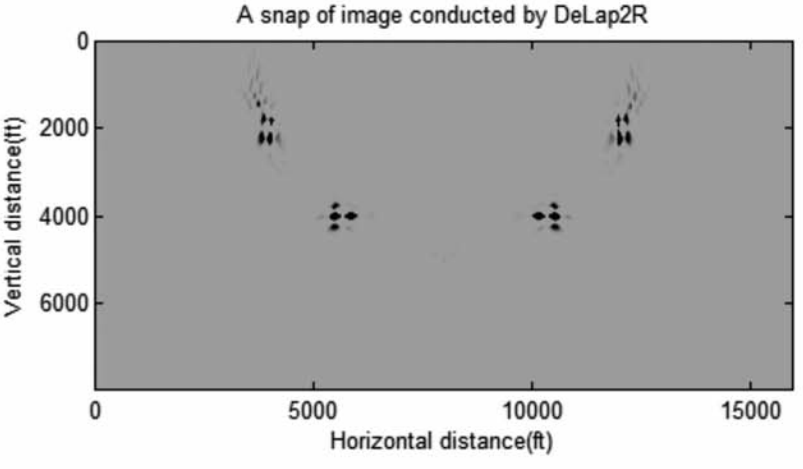

(b)

Fig. 6. Snapshots of images at time 0.7 s. (a) Image conducted by the zero-lag cross-correlation imaging condition; (b) image conducted by the second part of the decomposition of the Laplacian operator (*DeLap*2R).

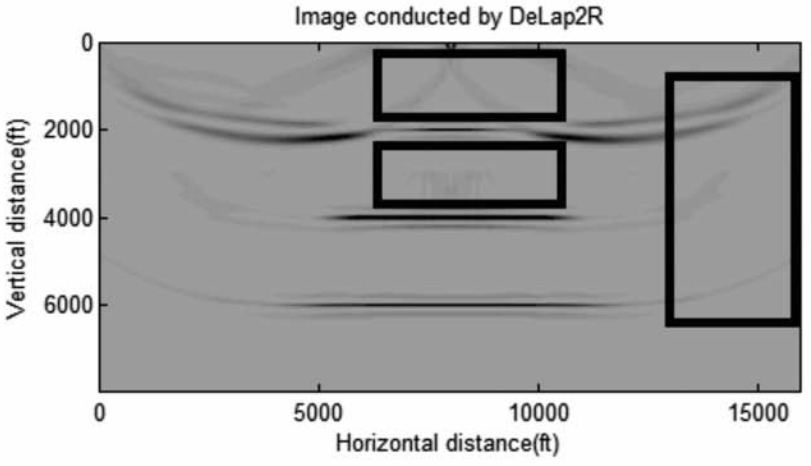

Fig. 7. Images conducted by *DeLap*2R for the 4-layer velocity model.

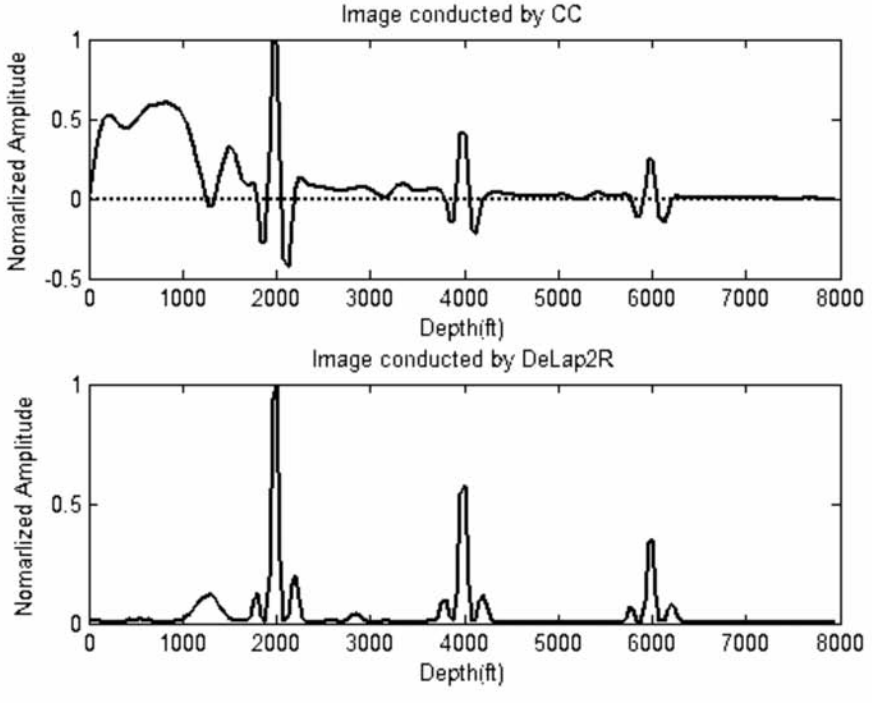

Fig. 8. Comparison between the images conducted by CC and *DeLap*2R on a vertical test line at horizontal distance 9000 ft, where these amplitudes are normalized by the maximum amplitude.

Synthetic numerical examples

We select Sigsbee2A synthetic model (Paffenholz et al., 2002) as another complex example to test the proposed imaging condition. Fig. 9 shows the velocity model. Three test zones are employed to verify the proposed imaging condition. Due to a large salt body in the model, strong back-scattering waves will cause artifacts and contaminate the final image. It challenges the imaging conditions.

To compare the performance of these imaging conditions in more challenging setting, no preconditions is used in this numerical simulation, such as deleting head waves and direct waves. Fig. 10 shows the images in the three zones conducted by CC and the proposed imaging condition. As shown in Figs. 10(a)-(b) and 10(c)-(d), the images conducted by the proposed imaging condition are more distinct than those conducted by CC. The interfaces of layers in the image conducted by *DeLap*2R are thinner than those conducted by CC. Furthermore, there are less artifacts and noises in the salt-body in the image conducted by *DeLap*2R. It verifies the conclusion drawn in the four-layer model again. The proposed imaging condition can reduce the artifacts between layers. Thus, we conclude that the proposed imaging condition is more effective for RTM and can form better images of layers.

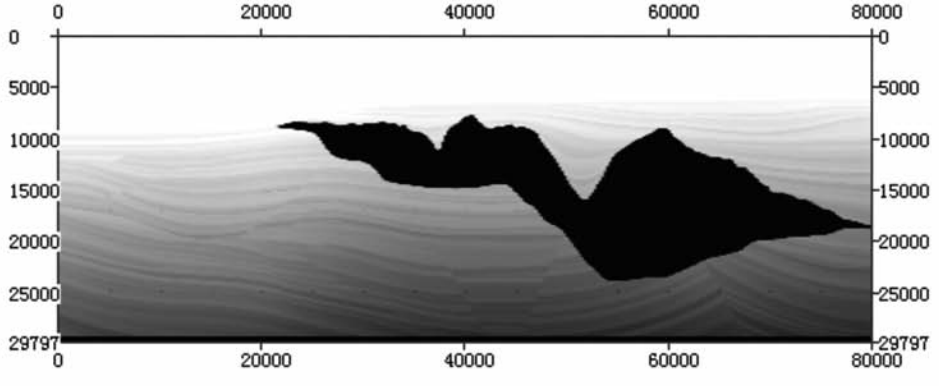

Fig. 9. Sigsbee2A velocity model.

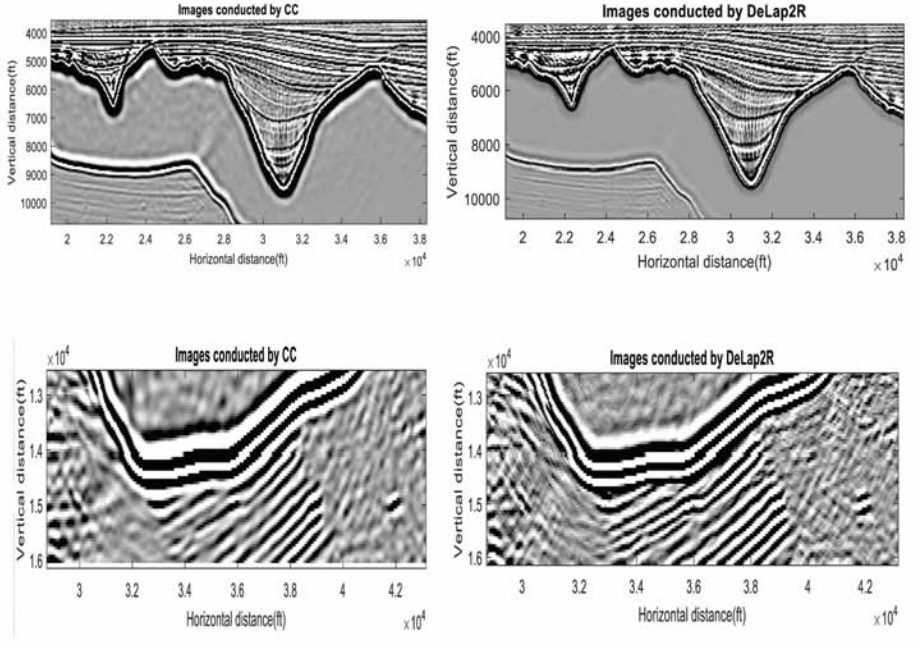

Fig. 10. Images conducted by zero-lag cross-correlation imaging condition (left) and the proposed imaging condition(right).

CONCLUSIONS

RTM is better than other imaging approaches for complex layers because it can simulate wave propagation without any approximations. However, RTM is criticized because it brings some artifacts. Laplacian operator is a traditional and effective approach to filtering images conducted by zero-lag cross-correlation imaging condition, which can significantly improve images. In this study, the basis of the improvement is demonstrated via a mathematical decomposition of Laplacian operator. Based on this decomposition, the effective part of Laplacian operator is identified, and a new imaging condition is proposed. The proposed image condition can image in the gradient domain and dampen artifacts in the angle domain, and it can remove most of noises in the images. The proposed imaging condition is easy to use, and only a small amount of additional computation is needed to form images. It can attenuate artifacts and significantly improve imaging quality. However, this decomposition has only been performed mathematically, and its dynamic meaning has not been analyzed and will be further researched in the future.

ACKNOWLEDGMENTS

This work was supported in part by the Innovation Team Fund of Southwest Petroleum University under Grant No. 2015CXTD07. We appreciate the assistance of Dr. Song.

REFERENCES

Baysal, E., Kosloff, D.D. and Sherwood, J.W.C., 1983. Reverse time migration. Geophysics, 48, 1514-1524.

Baysal, E., Kosloff, D.D. and Sherwood, J.W.C., 1984. A two-way nonreflecting wave equation: Geophysics, 49, 132-141.

Chattopadhyay, S. and McMechan, G.A., 2008. Imaging conditions for prestack reverse-time migration. Geophysics, 73(3): 81-89.

Claerbout, J.F., 1971. Toward a unified theory of reflector mapping: Geophysics, 36, 467-481.

Claerbout, J.F., 1985. Imaging the Earth's Interior. Blackwell Science Inc., Oxford.

Claerbout, J.F., 1998. Multidimensional recursive filters via a helix. Geophysics, 63: 1532-1541.

Costa, J.C., Silva, F.A., Alcantara, M.R., Schleicher, J. and Novais, A., 2009. Obliquity-correction imaging condition for reverse time migration. Geophysics, 74(3): S57-S66.

Diaz, E. and Sava, P., 2012. Understanding the reverse time migration backscattering: Noise or signal? Expanded Abstr., 82nd Ann. Internat. SEG Mtg., Las Vegas: 111-123.

Fei, T.W., Luo, Y. and Schuster, G.T., 2010. De-blending reverse-time migration. Expanded Abstr., 80th Ann. Internat. SEG Mtg., Denver: 3130-3134.

Feng, L.L, Yang, D.H. and Xie, W., 2015. An efficient symplectic reverse time migration method using a local nearly analytic discrete operator in acoustic transversely isotropic media with a vertical symmetry axis. Geophysics, 80: S103-S112.

Fletcher, R.F., Fowler, P., Kitchenside, P. and Albertin, U., 2005. Suppressing unwanted internal reflections in prestack reverse-time migration. Geophysics, 71(6): E79-E82.

Guitton, A., Kaelin, B. and Biondi, B., 2007. Least-square attenuation of reverse time migration artifacts. Geophysics, 72: S19-23.

Guitton, A., Valenciano, A., Sevc, D. and Clearbout J., 2007. Smoothing imaging condition for shot-profile migration. Geophysics, 72: 149-154.

Haney, M.M., Bartel, L.C., Aldridge, D.F. and Symons, N.P., 2005. Insight into the output of reverse-time migration. What do amplitudes mean? Expanded Abstr., 75th Ann. Internat. SEG Mtg., Houston: 1950-1953.

Kaelin, B. and Guitton, A., 2006. Imaging condition for reverse time migration. Expanded Abstr., 76th Ann. Internat. SEG Mtg., New Orleans: 2594-2598.

Li, J.S., Yang, D.H. and Liu, F.Q., 2013. An efficient reverse-time migration method using local nearly analytic discrete operator. Geophysics, 78(1): S15-S23.

Liu, F., Zhang, G.Q., Morton, S.A. and Leveille, J.P., 2008. An anti-dispersion wave equation for modeling and reverse time migration. Expanded Abstr., 78th Ann. Internat. SEG Mtg., Las Vegas: 277-2281.

Liu, F., Zhang, G.Q., Morton, S.A. and Leveille, J.P., 2007. Reverse time migration using one-way wavefield imaging condition. Expanded Abstr., 77th Ann. Internat. SEG Mtg., San Antonio, 36: 2170-2174.

Liu, F., Zhang, G.Q., Morton, S.A. and Leveille, J.P., 2011. An effective imaging condition for reverse-time migration using wavefield decomposition. Geophysics, 76: 29-39.

Loewenthal, D., Stoffa, P.L. and Faria, E.L., 1987. Suppressing the unwanted reflections of the full wave equation. Geophysics, 52: 1007-1012.

McMechan, G.G., 1983. Migration by extrapolation of time-dependent boundary values. Geophys. Prosp., 31: 413-420.

Mulder, W.A. and Plessix, R.E., 2003. One-way and two-way wave equation migration. Expanded Abstr., 80th Ann. Internat. SEG Mtg., 73rd Ann. Internat. SEG Mtg., Dallas: 881-884.

Paffenholz, J., McLain, B., Zaske, J. and Keliher, P., 2002. Subsalt multiple attenuation and imaging: Observations from the Sigsbee synthetic data set. Expanded Abstr., 72nd Ann. Internat. SEG Mtg., Salt Lake city: 2122-2125.

Pratt, W.K., 1978,. Digital Image Processing. Wiley Interscience., New York.

Ren, C.Y., Song, G.J. and Tian, X., 2015. The use of Poynting vector in wave-field decomposition imaging condition for reverse-time migration. J. Appl. Geophys., 112: 14-19.

Reuter, M., Biasotti, S., Giorgi, D., Patanè, G. and Spagnuolo, M., 2009. Discrete Laplace–Beltrami operators for shape analysis and segmentation. Comput. Graph., 33: 381-390.

Sava, P. and Fomel, S., 2006. Time-shift imaging condition in seismic migration. Geophysics, 71: 209-217.

Sava, P. and Vasconcelos, I., 2011. Extended imaging conditions for wave-equation migration. Geophys. Prosp., 59: 35-55.

Schuster, G.T. and Dai, W., 2010. Multi-source wave equation least-squares migration with a deblurring filter. Extended Abstr., 72nd EAGE Conf., Barcelona.

Suh, S.Y. and Cai, J., 2009. Reverse-time migration by fan filtering plus wave-field decomposition. Expanded Abstr., 79th Ann. Internat. SEG Mtg., Houston: 2804-2807.

Whitmore, N.D., 1983. Iterative depth migration by backward time propagation. Expanded Abstr., 53rd Ann. Internat. SEG Mtg. Las Vegas: 382-385.

Xie, W., Yang, D.H., Liu, F.Q. and Li, J.S., 2014. Reverse-time migration in acoustic VTI media using a high-order stereo operator. Geophysics, 79: WA3-WA11.

Yoon, K. and Marfurt, K.J., 2006. Reverse-time migration using the pointing vector. Explor. Geophys., 37: 102-107.

Youn, O. and Zhou, H.W., 2001. Depth imaging with multiples. Geophysics, 66: 246-255.

Yan, R. and Xie, X.B., 2009. A new angle-domain imaging condition for prestack reverse-time migration. Expanded Abstr., 79th Ann. Internat. SEG Mtg., Houston: 2784-2789.

Zhang, Y., Sheng, X., Bleistein, N. and Zhang, G., 2007. True amplitude, angle domain, common-image gathers from one-way wave equation migrations. Geophysics, 72: 49-58.

Zhang, Y. and Sun, J., 2009. Practical issues in reverse time migration: true amplitude gathers, noise removal and harmonic source encoding. First Break, 27: 53-59.

Zhou, M. and Schuster, G.T., 2002. Wave-equation wavefront migration. Expanded Abstr., 72nd Ann. Internat. SEG Mtg., Salt Lake City: 1292-1295.

APPENDIX

PROOF OF THE DECOMPOSITION OF THE LAPLACIAN OPERATOR FOR REVERSE TIME MIGRATION

Assume u and v are $u(x_1, x_2, \mathrm{L}\ , x_n)$ and $v(x_1, x_2, \mathrm{L}\ , x_n)$, respectively. For any x_i, the first and second differentials of u and v may be expressed as

$$\frac{\partial}{\partial x_i}(uv) = u_{x_i} v + u v_{x_i} \tag{A-1}$$

and

$$\frac{\partial^2}{\partial x_i^2}(uv) = u_{x_i x_i} v + 2u_{x_i} v_{x_i} + u v_{x_i x_i}, \tag{A-2}$$

respectively. Thus, the Laplacian operator of uv may be computed as

$$\begin{aligned} \nabla^2(uv) &= \sum_{i=1}^{n} \frac{\partial^2}{\partial x_i^2}(uv) \\ &= \nabla^2(u)v + 2\nabla u \cdot \nabla v + u\nabla^2(v) \\ &= \nabla^2(u,v)\cdot(v,u) + 2\nabla u \cdot \nabla v \end{aligned} \quad , \tag{A-3}$$

where ∇^2 and ∇ are the Laplacian operator and the gradient operator, respectively. $\nabla^2(u,v)$ is equal to $(\nabla^2 u, \nabla^2 v)$, and the symbol $\cdot$ is the inner product of vectors.

The scalar wave equation may be expressed as

$$u_{tt} = c^2 \nabla^2 u \quad , \tag{A-4}$$

where c is the sonic velocity of the media.

By inserting (A-4) into (A-3), we obtain

$$\nabla^2(uv) = c^2 \partial_{tt}(u,v)\cdot(u,v) + 2\nabla(u)\cdot\nabla(v) \quad , \tag{A-5}$$

where (u,v) is the vector comprising of u and v, and $\partial_{tt}(u,v) = (u_{tt}, v_{tt})$.